

Article

Green-Routed Carbon Dot-Adorned Silver Nanoparticles for the Catalytic Degradation of Organic Dyes

Suguna Perumal ^{1,†}, Thomas Nesakumar Jebakumar Immanuel Edison ^{2,†}, Raji Atchudan ^{3,*,†},
Ashok K. Sundramoorthy ^{4,†} and Yong Rok Lee ^{3,*}

¹ Department of Chemistry, Sejong University, Seoul 143747, Korea

² Department of Chemistry, Saveetha School of Engineering, Saveetha Institute of Medical and Technical Sciences, Chennai 602105, Tamil Nadu, India

³ School of Chemical Engineering, Yeungnam University, Gyeongsan 38541, Korea

⁴ Department of Prosthodontics, Saveetha Institute of Medical and Technical Sciences, Saveetha Dental College and Hospitals, Poonamallee High Road, Velappanchavadi, Chennai 600077, Tamil Nadu, India

* Correspondence: atchudanr@yu.ac.kr (R.A.); yrlee@yu.ac.kr (Y.R.L.)

† These authors contributed equally to this work.

Abstract: Herein, a simple, cost-effective, and in-situ environmentally friendly approach was adopted to synthesize carbon dot-adorned silver nanoparticles (CDs@AgNPs) from yellow myrobalan (*Terminalia chebula*) fruit using a hydrothermal treatment without any additional reducing and or stabilizing agents. The as-synthesized CDs@AgNP composite was systematically characterized using multiple analytical techniques: FESEM, TEM, XRD, Raman, ATR-FTIR, XPS, and UV-vis spectroscopy. All the results of the characterization techniques strongly support the idea that the CDs were successfully made to adorn the AgNPs. This effectively synthesized CDs@AgNP composite was applied as a catalyst for the degradation of organic dyes, including methylene blue (MB) and methyl orange (MO). The degradation results revealed that CDs@AgNPs exhibit a superior catalytic activity in the degradation of MB and MO in the presence of NaBH₄ (SB) under ambient temperatures. In total, 99.5 and 99.0% rates of degradation of MB and MO were observed using CDs@AgNP composite with SB, respectively. A plausible mechanism for the reductive degradation of MB and MO is discussed in detail. Moreover, the CDs@AgNP composite has great potential for wastewater treatment applications.

Keywords: *Terminalia chebula*; silver nanoparticles; catalytic degradation; methylene blue; methyl orange; organic dyes



Citation: Perumal, S.; Edison, T.N.J.I.; Atchudan, R.; Sundramoorthy, A.K.; Lee, Y.R. Green-Routed Carbon Dot-Adorned Silver Nanoparticles for the Catalytic Degradation of Organic Dyes. *Catalysts* **2022**, *12*, 937. <https://doi.org/10.3390/catal12090937>

Academic Editors: Sekar Karthikeyan and Boopathy Ramasamy

Received: 27 July 2022

Accepted: 19 August 2022

Published: 24 August 2022

Publisher's Note: MDPI stays neutral with regard to jurisdictional claims in published maps and institutional affiliations.



Copyright: © 2022 by the authors. Licensee MDPI, Basel, Switzerland. This article is an open access article distributed under the terms and conditions of the Creative Commons Attribution (CC BY) license (<https://creativecommons.org/licenses/by/4.0/>).

1. Introduction

Today, nanomaterials with different architecture and supports play key roles in industrial catalysis. They provide exciting opportunities for dealing with various chemical transformations and environmental challenges [1–5]. The catalytic processes are mainly classified into three categories, including homogeneous, heterogeneous, and enzyme/biocatalysis, which are based on the phase nature of the catalyst [6,7]. Among these, the heterogeneous catalytic process is industrially and environmentally important due to its application in biologically important chemical transformations and environmental remedies such as dye degradation, pesticide removal, and photocatalytic dye degradation [8–11]. Generally, heterogeneous catalysts are solid materials that increase the rate of a chemical reaction and remain unchanged after the completion of the reaction. The unchanged catalysts can be quickly recovered and recycled. Thus, dye degradation with the help of heterogeneous catalysts is an interesting topic among environmental scientists. Based on reports, noble metal nanoparticles, such as gold, silver, and palladium nanoparticles, show excellent catalytic activities in the reduction/degradation of toxic dyes by aqueous sodium borohydride

(SB) [12–14]. However, the stability of these nanoparticles is limited, and, hence, carbon-supported noble metal nanoparticles have been developed as catalysts for the reduction of dyes and dye effluents, which are highly stable and easily recoverable [15]. Among these metal nanoparticles, silver nanoparticles (AgNPs) are considered valuable for their high electrical conductivity, low cost, and high catalytic activity [16–19]. Carbon-supported AgNPs can be synthesized by various methods, including organometallic grafting, ion exchange, and the hydrothermal method combined with the reduction of silver ions, where the hydrothermal-assisted reduction method provides diverse advantages, such as easy setup, cost-effectiveness, and high stability compared to the other reported methods [20–22]. Methylene blue (MB) and methyl orange (MO) are the two important industrial organic dyes applied in the printing and textile dyeing industries. Therefore, the waste effluents of these industries mainly contain MB and MO. High-level exposure to these dyes causes various illness in human beings and also other living things [23–25]. Thus the degradation/reduction of MB and MO is significant [26].

Hence, the main aim of this work was to synthesize carbon dot-adorned silver nanoparticles with the benefits of cost-effectiveness and a greener route of synthesis. *Terminalia chebula* fruits were utilized as the base material for the synthesis of the carbon dots, as well as the reducing agent for turning the silver nitrate (AgNO_3) into AgNPs. This is a route for the concurrent synthesis of the carbon dots decorated with silver nanoparticles (CDs@AgNPs). The resulted CDs@AgNP composite was characterized in detail using various physicochemical techniques to confirm their structure and compositions. Then, the structural confirmed CDs@AgNP composite was utilized as a potential heterogeneous catalyst for the reductive degradation of organic dyes, including MB and MO, in the presence of SB (NaBH_4). The degradation of the organic dyes in the presence and absence of the catalyst (CDs@AgNP composite) and SB was examined, and the corresponding results were discussed. All the results suggested that the CDs@AgNP composite acted as the best catalyst for the degradation of MB and MO.

2. Results and Discussion

2.1. Structural Characterization of the Synthesized CDs@AgNPs Composite

The structural and chemical compositions of the prepared CDs@AgNP composite were characterized by various techniques, such as XRD, Raman, FESEM, TEM, ATR-FTIR, and XPS. The optical properties of the CDs@AgNPs were studied using the UV-vis spectrum. The absorption spectra of the fruit extract and CDs@AgNPs are shown in Figure S1. After the hydrothermal process, the color of the resultant solution changed from pale yellow to brownish yellow, which indicated the formation of the CDs@AgNP composite [27]. The photographic images of the TCE and CDs@AgNP aqueous solutions are displayed in the inset of Figure S1. The TCE exhibited a base peak at 280 nm respective to the π - π^* electronic transition of the carbonyl phytoconstituents (tannin) of *Terminalia chebula*. The CDs@AgNP composite showed a sharp and clear surface plasmon resonance absorbance peak at 425 nm and a shoulder peak at 380 nm. A peak at 425 nm confirmed the formation of the AgNPs [28,29]. Further, the TCE peak intensity decreased and slightly shifted towards a higher wavelength, rising to 320 nm from 280 nm in the CDs@AgNPs. This might be due to the carbonization and complete reduction of the tannins present in the extract. These results revealed the presence of C=C and C=O bonds in the prepared CDs@AgNPs.

The crystal structure of the CDs@AgNPs was characterized by XRD. As shown in Figure 1a, the XRD pattern exhibited four sharp peaks, with the 2θ values of 38.1, 44.2, 64.4, and 76.4°, which are related to the (111), (200), (220), and (311) planes of the AgNPs [30]. This XRD results confirmed the presence of AgNPs in the prepared CDs@AgNPs. However, patterns responsible for the CDs were missing. This could be because of the high intensity of the patterns that correspond to the AgNPs, but the observation of CD patterns was not possible. Further, the CDs@AgNPs were characterized using Raman spectroscopy (Figure 1b). In contrast to the XRD results, Raman studies revealed the presence of CDs and AgNPs in the CDs@AgNPs. The Raman spectrum of the CDs@AgNPs showed

four predominant peaks. The peaks at 1350, 1575, and 2800 cm^{-1} are contributed by the D, G, and 2D bands of CDs, being typical peaks of a graphitic carbon structure [31,32]. The peaks between 350 and 750 cm^{-1} are responsible for the AgNPs.

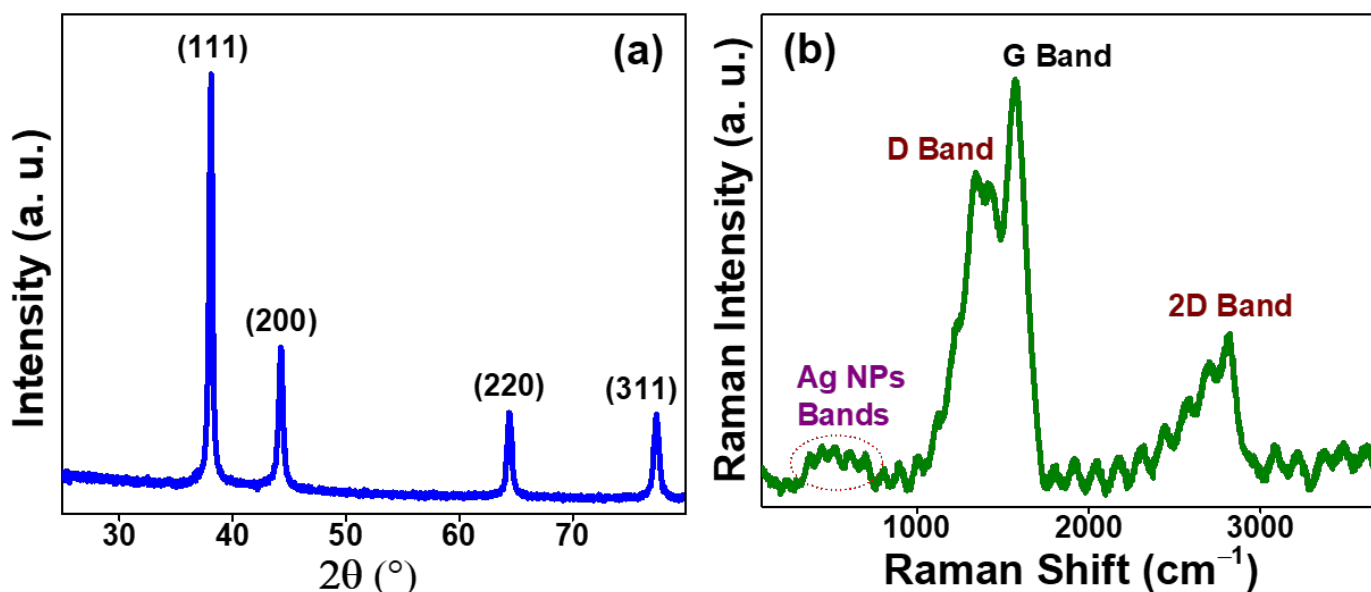


Figure 1. (a) XRD pattern and (b) Raman spectrum of the synthesized CDs@AgNPs.

Figure 2 shows the FESEM images of the prepared CDs@AgNPs with different magnifications. The irregular morphologies of the CDs@AgNPs in the hierarchical process can be observed (Figure 2a–d). This is because of the very small size of the CDs and AgNPs. However, the elements present in CDs@AgNPs were demonstrated using elemental mapping images (Figure 2e–i). This directly indicated that the carbon (C), oxygen (O), nitrogen (N), and silver (Ag) were homogeneously distributed in the CDs@AgNPs. Furthermore, the uniform distribution of C, O, N, and Ag elements is revealed by Figure 2i. The C, O, and N elements in the CDs@AgNPs derive from the plant source, and the element Ag is derived from the AgNO_3 . Moreover, the EDAX spectrum in Figure S2 revealed the presence of the elements C, N, O, and Ag in CDs@AgNPs, along with the platinum and silicon signals that were used for the sputter coating and crystalline silicon wafer substrate, respectively.

Consistent with the FESEM results, the TEM/HRTEM observation of the CDs@AgNPs, as indicated by Figure 3, led to the discovery of the irregular morphology of the CDs. The presence of CDs on the AgNP surface is evident from Figure 3a–e. The HRTEM showed that the carbon lattice was enclosed on the AgNPs. The size distribution histogram of the AgNPs (inset Figure 3c) was obtained by measuring the sizes of 100 randomly selected nanoparticles from the TEM image (Figure 3b). The average AgNP size in the CDs@AgNP composite was about 20 nm. Furthermore, the HETRM images revealed the spherically shaped AgNPs, and the particle size was calculated at about 20 nm and was relatively uniform. The AgNPs had a fine fringe pattern, with a spacing of 0.24 nm, corresponding to the Ag (111) lattice fringes (Figure 3e). The HRTEM image also showed visible crystalline lattice fringes, with bright spots in the selected area electron diffraction (SAED) pattern. This SAED in Figure 3f indicates the crystalline nature of the CDs@AgNPs.

Furthermore, an ATR-FTIR study was performed to identify the functional groups that were present in the CDs@AgNPs (Figure S3). The spectra of the TCE showed a broad peak centered at 3250 cm^{-1} , revealing the presence of O–H/N–H bonds. The peaks at 2850 and 2920 cm^{-1} occurred due to the C–H antisymmetric and symmetric bonds, respectively. The intense peaks at 1620 and 1050 cm^{-1} are responsible for the stretching vibrations of the C=O/C=C and C–O–C bonds, respectively. For the CDs@AgNPs, the broad peaks between 3500 and 3100 cm^{-1} are responsible for the O–H/N–H bonds [33]. The C–H stretching vibration was observed at 2870 cm^{-1} from the graphitic structure of the CDs@AgNPs [34].

A strong peak at 1650 cm^{-1} was attributed to the C=O/C–C vibrations. The C–N and O–H/N–H/C–OH bonds can be observed at 1430 and 1314 cm^{-1} , respectively [35]. The peaks at 1050 and 826 cm^{-1} are responsible for the C–O–C and –CH₂ groups in the CDs@AgNPs, respectively [36]. The presence of the AgNPs confirms the peak at 480 cm^{-1} . These results reveal that the CDs@AgNPs were rich in oxygen and nitrogen functional groups, such as hydroxyl, carbonyl, carboxylic acid, amide, and amino groups. These nitrogen functional groups could serve as stabilizing agents for the AgNPs.

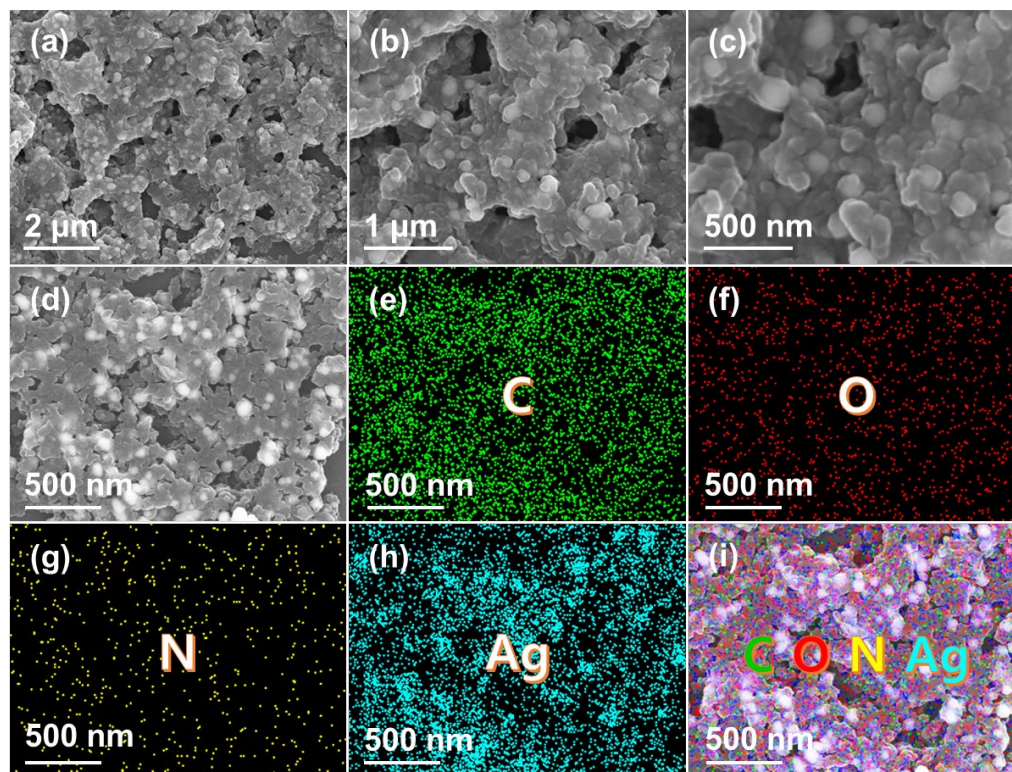


Figure 2. (a–c) FESEM images of the synthesized CDs@AgNPs; (d) FESEM electron image and (e–h) the corresponding elemental mapping; and (i) overlapping image of all elements (d–h) of the synthesized CDs@AgNPs.

XPS measurements were carried out to investigate the chemical compositions and elemental states of the CDs@AgNPs. As shown in Figure S4, the survey spectrum disclosed four peaks: C 1s at 285 eV, Ag 3d at 368 eV, N 1s at 400 eV, and O 1s at 533 eV. Thus, the prepared CDs@AgNPs were composed of the elements C, O, Ag, and N, with values of 60, 27, 7, and 6% (inset of Figure S4). The high-resolution spectrum of C 1s (Figure 4a) resulted in four peaks at 284.8, 286.0, 287.2, and 288.9 eV, which can be assigned to C=C/C–C, C–N/C–O, C=O/C=N, and HO–C=O, respectively [37]. The C=C/C–C peak corresponds to the presence of sp² graphitic/sp³ hybrid structures in the CDs@AgNPs [38]. The reduction process of the AgNO₃, resulting in the formation of AgNPs, was confirmed by the existence of a peak at the Ag 3d level [39]. With respect to the deconvolution of the Ag 3d level results, two peaks at 368.1 and 374.2 eV can be attributed to the 3d_{5/2} and 3d_{3/2}, respectively (Figure 4b). This indicated the presence of metallic Ag in the CDs@AgNPs [27,39]. Figure 4c shows the deconvolution spectrum of the N 1s level that resulted in three peaks at 399.0, 400.0, and 401.6 eV, which can be assigned to C–N–C, C–N–H, and (C)₃–N, respectively. The O 1s spectrum (Figure 4d) reveals the presence of O atoms in the C=O at 531.4 eV, C–O–C/C–OH at 532.4 eV, and HO–C=O at 533.4 eV [40]. The XPS showed results consistent with those of the ATR-FTIR, and, thus, the overall results of the XPS and ATR-FTIR validate and confirm that the CDs@AgNPs consisted of many functional groups, such as carboxyl, hydroxyl, amide, amino, and carbonyl groups.

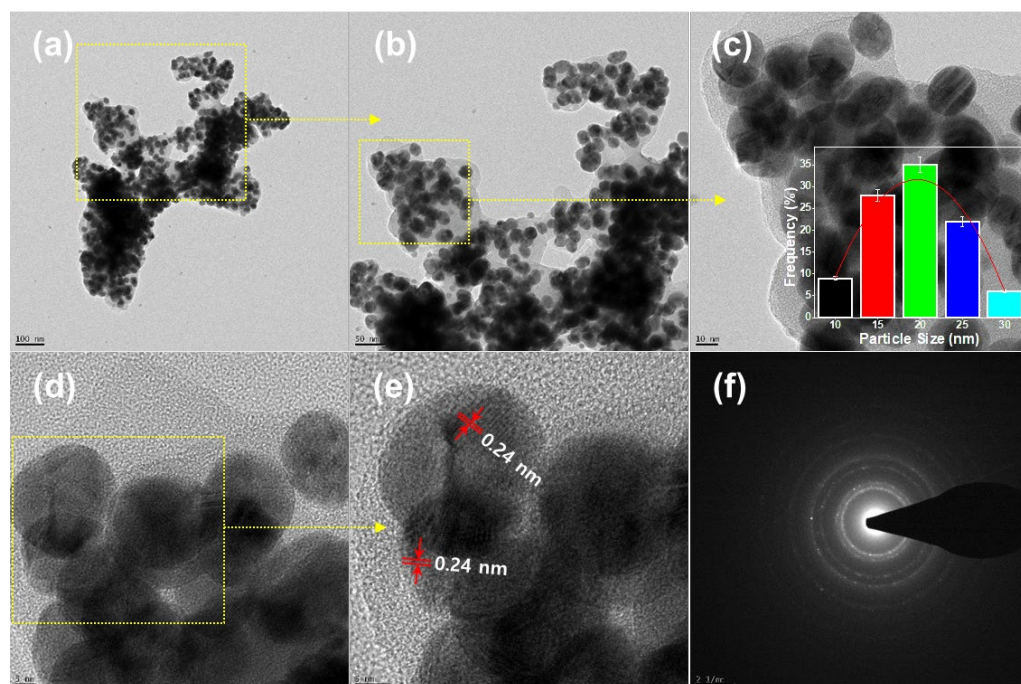


Figure 3. (a–e) TEM/HRTEM images and (f) the corresponding SAED pattern of the synthesized CDs@AgNPs (inset (c) is the particle size distribution graph of the CDs@AgNPs).

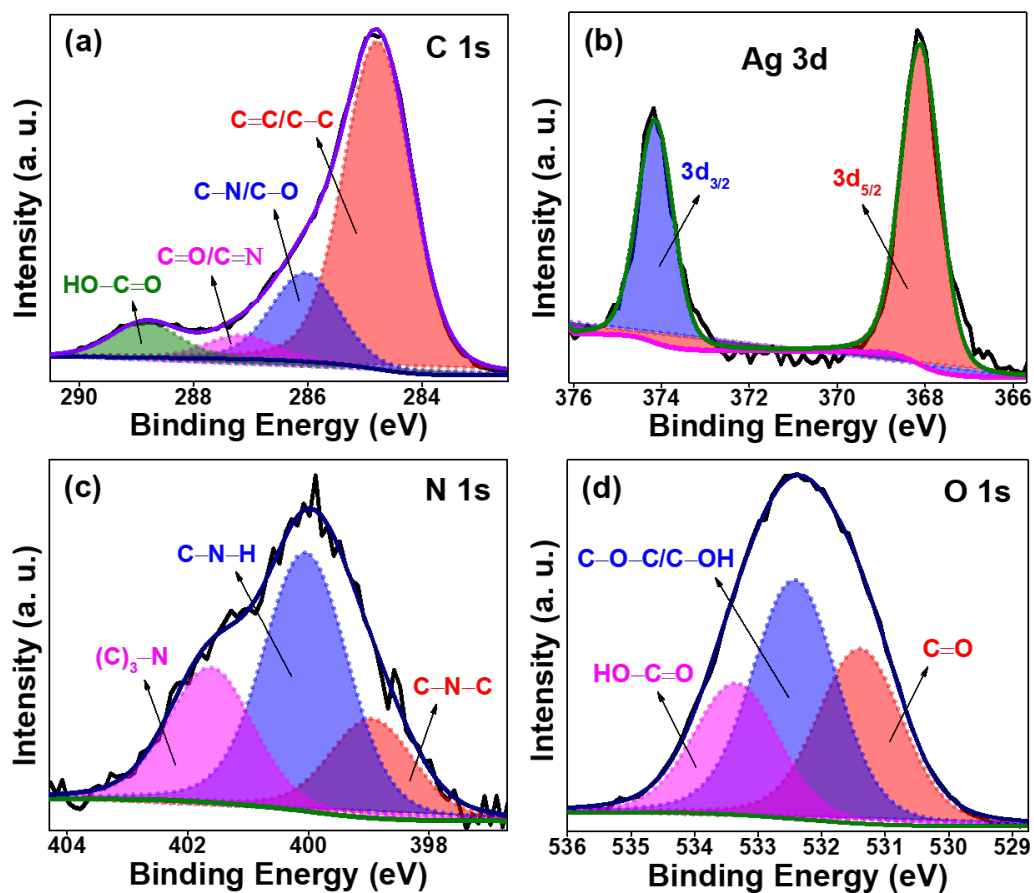


Figure 4. High-resolution XPS spectra (a) C 1 s, (b) Ag 3 d, (c) N 1 s, and (d) O 1 s of the synthesized CDs@AgNPs.

2.2. Catalytic Activity of the Synthesized CDs@AgNPs Composite towards the Degradation of Organic Dyes

The catalytic performance of the CDs@AgNP composite was studied in terms of the reductive degradation of MB and MO using aqueous SB solution. The catalytic activity of the CDs@AgNP composite was monitored through visual observation and also by using UV-vis spectroscopy. In order to confirm the catalytic ability of the CDs@AgNP composite, as a control experiment, degradations of MB and MO without the CDs@AgNP composite were conducted. Figures S5–S8 show the UV-vis absorbance spectra of the MB/MO in the presence of SB (and in the absence of CDs@AgNPs) and in the presence of CDs@AgNPs (and in the absence of SB), respectively. In these control experiments, insignificant changes in the characteristic absorbance peaks for MB and MO, centered at 665 and 465 nm, were observed, respectively. This suggests that the degradation of MO and MB does not only occur when using a catalyst (the CDs@AgNP composite) or the reductive agent SB.

Conversely, after mixing SB and CDs@AgNPs and their application to MB/MO, the reductive degradation reaction commenced quickly with the evolution of the hydrogen gas, which was identified from the color degradation and decrement in the absorbance intensity, as exhibited by the respective time-dependent UV-vis spectra in Figure 5a,b. This result confirmed the catalytic activity of the CDs@AgNPs in the degradation of MB and MO [41–43]. Furthermore, the level of degradation (%) and rate of reaction as per the pseudo-first-order kinetic model for both MB and MO were calculated. The achieved degradation levels for the MB and MO dyes were about 99.5 and 99.0%, respectively (Figure 5c). Figure 5d shows the degradation time vs. $\ln(A_t/A_0)$ kinetic graphs of MB and MO. It is noticeable that the kinetic graphs of MB and MO yielded linear straight lines with rate constants (slope values) of 0.204 and 0.128 min^{-1} , and the respective linearity coefficient (R^2) values were about 0.985 and 0.986, respectively. This result suggests that the degradation of MB/MO by the CDs@AgNP composite followed pseudo-first-order kinetics [44,45]. These catalytic reduction reactions can be explained using the Langmuir–Hinshelwood model. In this model, SB acts as an electron donor and hydrogen provider. After the addition of SB to the reaction, the pH of the solution changed to basic, and hence the surface charge of CDs@AgNP composite was changed to positive. Thus, the MB/MO and BH_4^- ions were concurrently adsorbed on the surface of the CDs@AgNP composite. Furthermore, the reduction reaction was initiated by relaying electrons from the donor BH_4^- ions acting as electron transfer mediators to the adsorbed MB/MO molecules through the CDs@AgNP composite. This was evident from the strong effervescence of the hydrogen gas that evolved, and, subsequently, this action led to the reductive degradation of MB and MO [46,47]. Furthermore, the visual observations of the MB/MO degradation in the presence of the CDs@AgNP composites with SB are shown in Figure 6. One can note the decoloring of the MB/MO aqueous solution by increasing the reaction time. The decoloring starts within 1 min, and complete decoloring (degradation product-DP) of the MB and MO was observed within 15 and 20 min, respectively. These photographic images confirm the effectiveness of the CDs@AgNP composite as a catalyst for the degradation of MB/MO. In order to ensure the greater activity of the prepared CDs@AgNP composite, the results of the present work were compared with the recent literature studies on MB/MO degradation by AgNPs-related composites, and the corresponding results are illustrated in Table 1. The CDs@AgNP composite achieved the degradation efficiency rates of 99.5 and 99.0% at the reaction times of 15 and 20 min, with the rate constants of 0.204 and 0.128 min^{-1} for the MB and MO, respectively, results which are significantly comparable with those of the performances of previously reported Ag-based catalysts [17,44,48–53]. This suggests that the CDs@AgNP composite exerted a high catalytic activity on the MB and MO in the aqueous medium under atmospheric conditions.

Furthermore, the FESEM images were captured and EDAX elemental mapping analyses of CDs@AgNP composite were performed after the degradation of the organic dyes, and the corresponding results are shown in Figure S9. The FESEM image of the CDs@AgNP composite revealed the spherical shape of the AgNPs, and one can see that the particles

were relatively uniform in shape, with minute variation in size (Figure S9a). The elemental composition of the CDs@AgNP composite was examined by elemental mapping. The elemental mapping results of the CDs@AgNP composite confirmed that the concentrations of the different elements, including C, O, N, and Ag, were uniform in the composite (Figure S9b–e). Furthermore, the uniform distribution of the C, O, N, and Ag elements was revealed by overlapping elemental mapping, as shown in Figure S9f. Hence, we could observe an insignificant amount of AgNPs leaching from the CDs@AgNP composite after the degradation of the organic dyes.

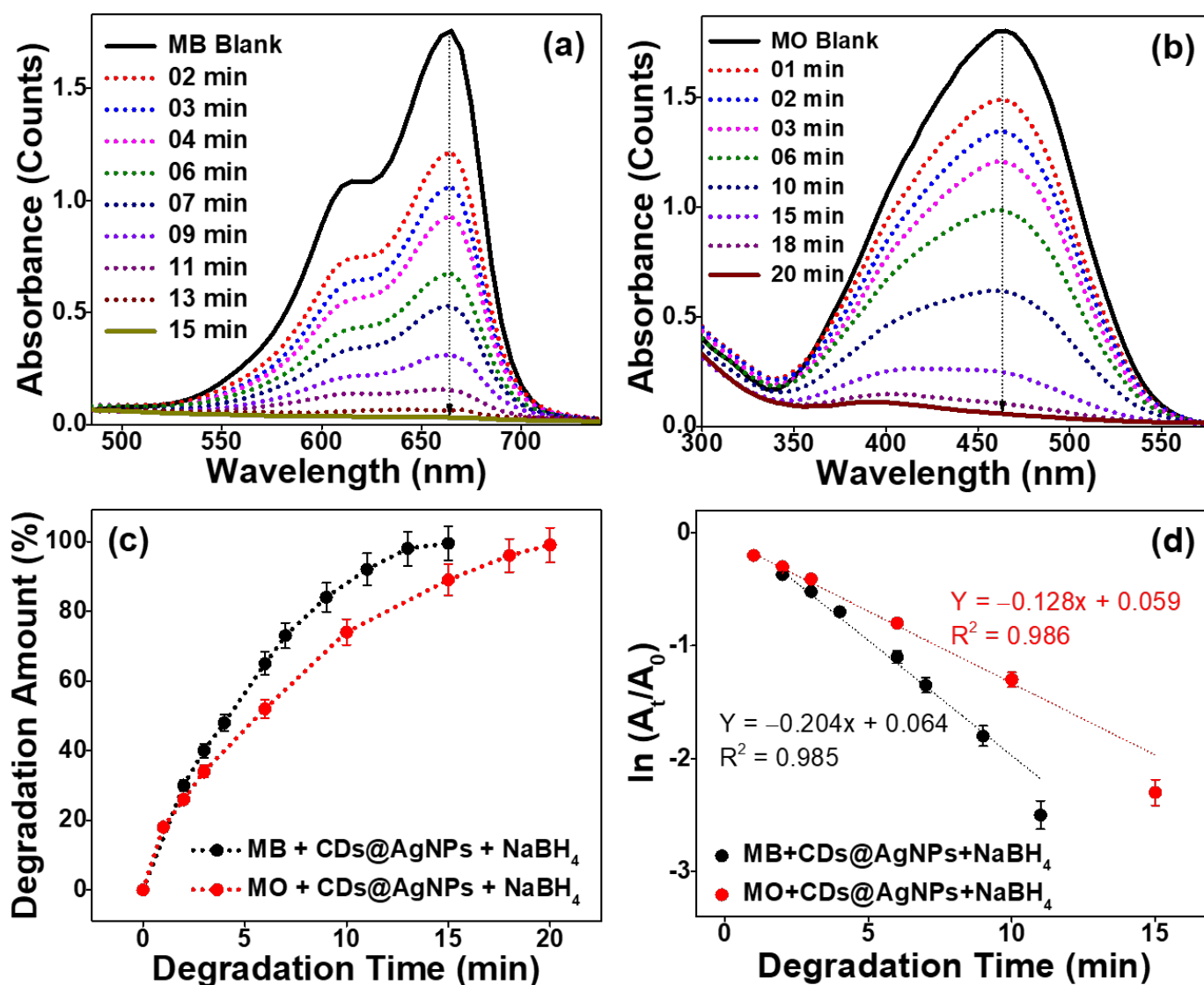


Figure 5. UV-vis absorbance spectra of (a) MB and (b) MO aqueous solutions in the presence of the CDs@AgNP composite and NaBH₄ at different degradation times, (c) degradation efficiencies (%) of the synthesized CDs@AgNP composite against MB and MO dye solutions, and (d) pseudo-first-order kinetic plots of the degradation of the MB and MO dyes.

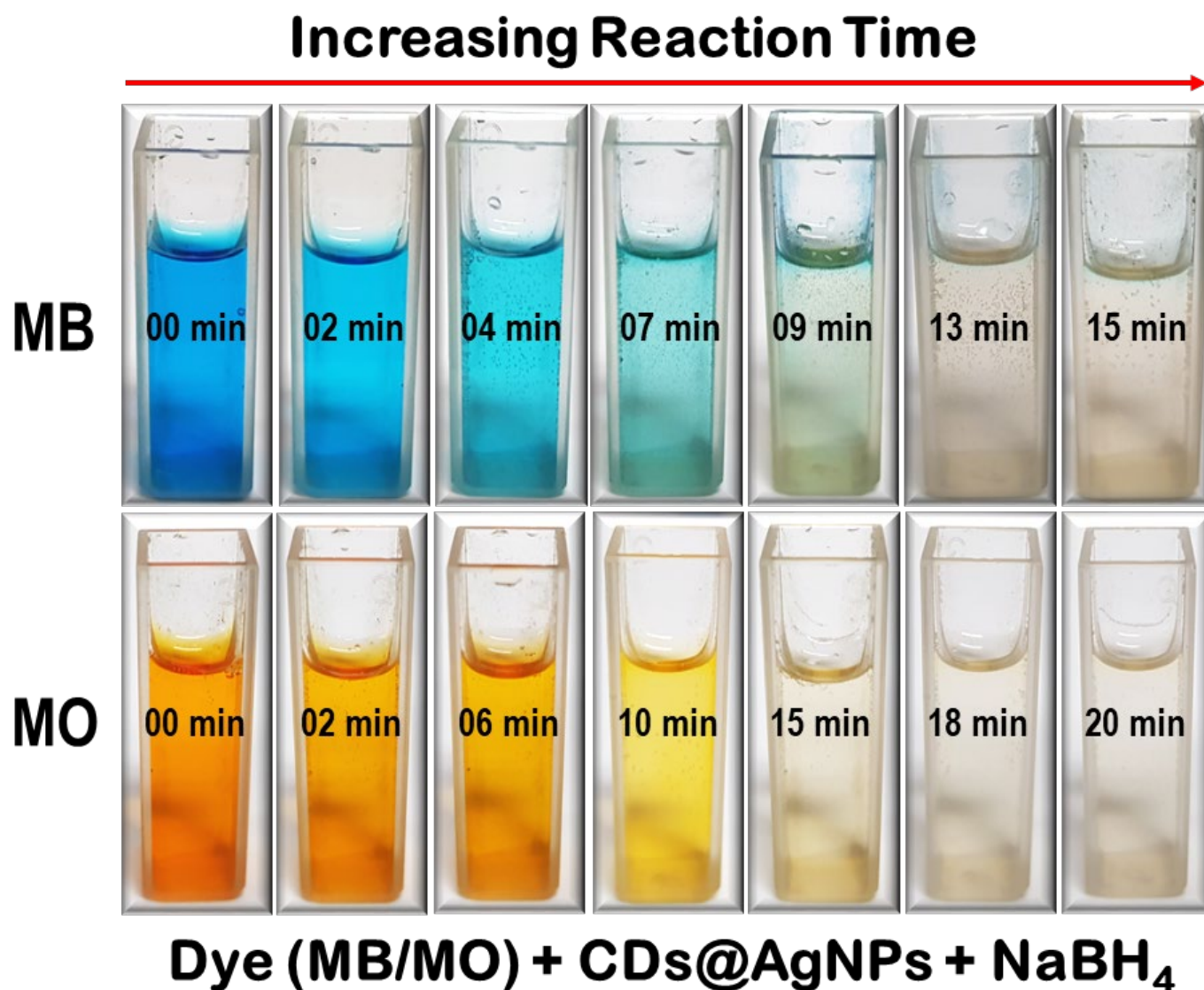


Figure 6. Photographic images of the MB and MO aqueous solutions with the CDs@AgNP composite in the presence of NaBH₄ at different reaction (degradation) times under ambient conditions.

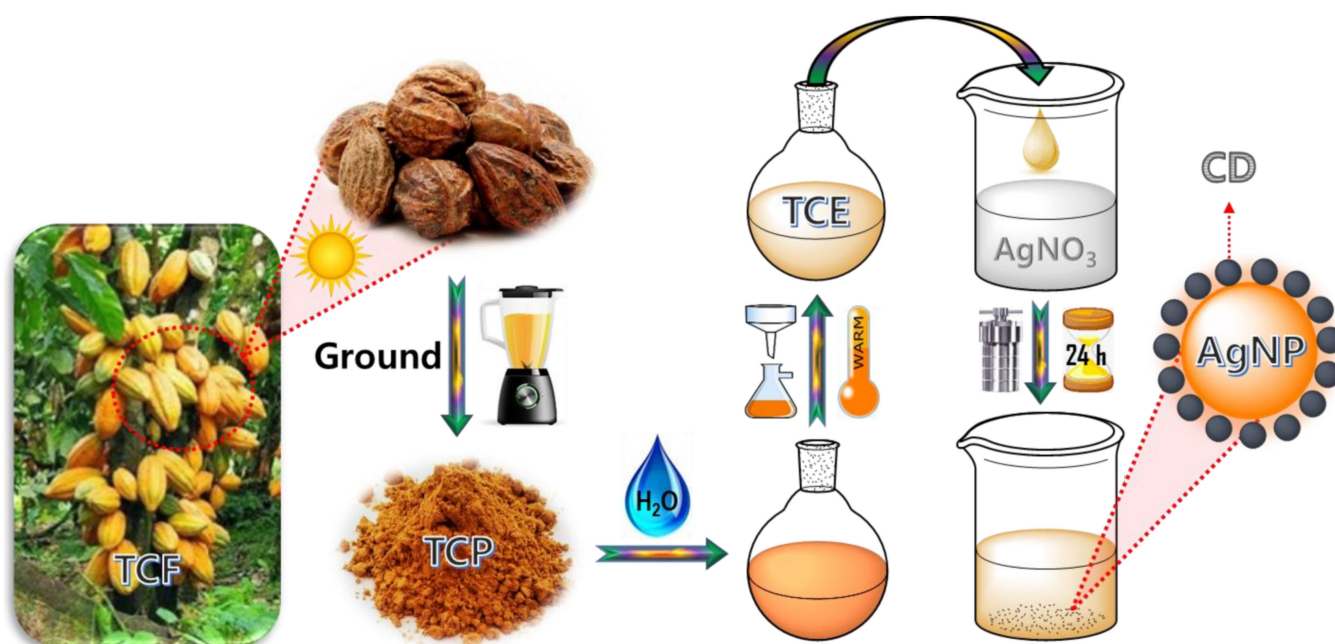
Table 1. Comparison of the catalytic performances of AgNP-based composites from bio-sources.

Catalyst	Reaction Time (min)	MB/MO Degradation (%)	Rate Constant (k)	Reference
Ag/Au composite	20	-(MB)	0.668 min ⁻¹	[48]
AgNPs/ <i>G. arborea</i>	10	100 (MB)	-	[17]
Ag NPs/peach kernel	10/12	100 (MB/MO)	-	[49]
Ag NPs/ <i>C. arvensis</i>	20	-(MB)	0.108 min ⁻¹	[50]
AS-AgNPs	27	97 (MB)	0.0007 s ⁻¹	[13]
AgNPs/Marine algae	20	99 (MB)	0.106 min ⁻¹	[44]
AgNPs-GS	60	94 (MO)	0.0725 min ⁻¹	[51]
AgNPs/PDS	40	88 (MO)	0.00159 s ⁻¹	[52]
Ag-ZX	25	100 (MO)	0.305 min ⁻¹	[53]
CDs@AgNPs	15/20 min	95.5/99.0	0.204/0.128 min ⁻¹	This work

3. Materials and Methods

Synthesis of the CDs@AgNP Composite

Terminalia chebula fruits were dried in sunlight followed crushing into a powder using a blender. To every 1 g of powder, 100 mL of distilled water was added and heated at 70 °C overnight. The mixture was cooled down and filtered using filter paper. In an autoclave reactor, 5 mL of the filtered mixture and 50 mL of 0.01 M AgNO₃ were taken and reacted at 200 °C for 24 h. After the reaction time, the mixture was cooled down and dried using a freeze-dryer. The dried CDs@AgNP composite was utilized for the characterization using X-ray diffractometry (XRD), Raman and field emission scanning electron microscopy (FESEM) together with energy-dispersive X-ray (EDX) spectroscopy, high-resolution transmission electron microscopy (HRTEM), attenuated total reflection Fourier-transform infrared spectroscopy (ATR-FTIR), and X-ray photoelectron spectroscopy (XPS). For the degradation analyses, the mixture was used as it is before drying. Scheme 1 illustrates the formation of the CDs@AgNP composite from the *Terminalia chebula* fruits extract (TCE) and AgNO₃ aqueous solution by a simple one-pot hydrothermal method.



Scheme 1. Formation of the CDs@AgNP composite from the *Terminalia chebula* fruit and silver nitrate via the one-step hydrothermal method.

4. Conclusions

In summary, a simple and effective CDs@AgNP catalyst was hydrothermally developed via a simple one-pot route as a catalyst for the reductive degradation of organic dyes, including MB and MO. From the ATR-FTIR spectra, we discovered that the plant extract could reduce and stabilize to form AgNPs, and the strong UV-vis absorbance of the final product confirmed the formation of the AgNPs. Excellent crystallinity and spherical-shaped morphology, with a lattice distance of 0.24 nm, were observed from the XRD, FESEM, and TEM/HRTEM analyses. The EDAX and XPS results demonstrated the presence of C, N, O, and Ag constituents in the synthesized CDs@AgNP composite. The XPS results revealed the characteristic peak of the Ag and the surface functionalities of oxygen- and nitrogen-presented moieties from the TCE. Furthermore, the ATR-FTIR and XPS revealed functional groups, such as hydroxyl, carbonyl, carboxyl, amide, and amino groups, in the CDs@AgNPs. The reductive catalytic activities of the CDs@AgNP composite in the presence of SB against degradation of MB and MO under ambient conditions were measured as 99.5 and 99.0% within 15 and 20 min, respectively. This degradation followed pseudo-first-order kinetics. The kinetic graphs of MB and MO dye yielded linear straight

lines, showing rate constants of 0.204 and 0.128 min⁻¹, with R² values of 0.985 and 0.986, respectively. Thus, the present study suggested that the TCE-assisted CDs@AgNP composite has potential as a reductive catalysts for the degradation of various organic dyes and could act as a nano-catalyst in other applications.

Supplementary Materials: The following supporting information can be downloaded at <https://www.mdpi.com/article/10.3390/catal12090937/s1>, Materials, instrumentation methods, and catalytic degradation measurement of the synthesized CDs@AgNPs, Figure S1. UV-vis spectra of the *Terminalia chebula* fruit extract and synthesized CDs@AgNPs, Figure S2. EDAX spectrum of the synthesized CDs@AgNPs, Figure S3. ATR-FTIR spectra of the *Terminalia chebula* fruit extract and synthesized CDs@AgNPs, Figure S4. XPS survey spectrum of the synthesized CDs@AgNPs, and the inset is a pie chart of the elemental composition of the synthesized CDs@AgNPs, Figure S5. UV-vis absorbance spectra of MB in the presence of SB at different reaction times, Figure S6. UV-vis absorbance spectra of MB in the presence of CDs@AgNPs at different reaction times, Figure S7. UV-vis absorbance spectra of MO in the presence of SB at different reaction times, Figure S8. UV-vis absorbance spectra of MO in the presence of CDs@AgNPs at different reaction times, Figure S9. (a) FESEM electron image and (b–e) the corresponding elemental mapping of (b) carbon, (c) oxygen, (d) nitrogen, and (e) silver in the CDs@AgNPs after the degradation of organic dyes; (f) overlapping image of all elements (a–e) of the CDs@AgNPs after the degradation of organic dyes.

Author Contributions: Visualization, and writing—review & editing, S.P.; investigation and writing—original draft, T.N.J.I.E.; conceptualization, data curation, formal analysis, investigation, and writing—original draft, R.A.; investigation and visualization, A.K.S.; project administration and supervision, Y.R.L. All authors equally contributed to this work. All authors have read and agreed to the published version of the manuscript.

Funding: This work was supported by the National Research Foundation of Korea (NRF) grant, funded by the Korean government MSIT (2021R1A2B5B02002436).

Acknowledgments: The authors thank the National Research Foundation of Korea (NRF) for providing financial support.

Conflicts of Interest: The authors declare no conflict of interest.

References

1. Mitchell, S.; Qin, R.; Zheng, N.; Pérez-Ramírez, J. Nanoscale engineering of catalytic materials for sustainable technologies. *Nat. Nanotechnol.* **2021**, *16*, 129–139. [[CrossRef](#)] [[PubMed](#)]
2. Chadha, U.; Selvaraj, S.K.; Ashokan, H.; Hariharan, S.P.; Mathew Paul, V.; Venkatarangan, V.; Paramasivam, V. Complex Nanomaterials in Catalysis for Chemically Significant Applications: From Synthesis and Hydrocarbon Processing to Renewable Energy Applications. *Adv. Mater. Sci. Eng.* **2022**, *2022*, 1552334. [[CrossRef](#)]
3. Li, J.; Ma, C.; Zhu, S.; Yu, F.; Dai, B.; Yang, D. A Review of Recent Advances of Dielectric Barrier Discharge Plasma in Catalysis. *Nanomaterials* **2019**, *9*, 1428. [[CrossRef](#)] [[PubMed](#)]
4. Liu, L.; Corma, A. Metal Catalysts for Heterogeneous Catalysis: From Single Atoms to Nanoclusters and Nanoparticles. *Chem. Rev.* **2018**, *118*, 4981–5079. [[CrossRef](#)]
5. Priyadharsan, A.; Vasanthakumar, V.; Karthikeyan, S.; Raj, V.; Shanavas, S.; Anbarasan, P.M. Multi-functional properties of ternary CeO₂/SnO₂/rGO nanocomposites: Visible light driven photocatalyst and heavy metal removal. *J. Photochem. Photobiol. A Chem.* **2017**, *346*, 32–45. [[CrossRef](#)]
6. Ye, R.; Hurlburt, T.J.; Sabyrov, K.; Alayoglu, S.; Somorjai, G.A. Molecular catalysis science: Perspective on unifying the fields of catalysis. *Proc. Natl. Acad. Sci. USA* **2016**, *113*, 5159–5166. [[CrossRef](#)]
7. Thongam, D.D.; Chaturvedi, H. Advances in nanomaterials for heterogeneous photocatalysis. *Nano Express* **2021**, *2*, 012005. [[CrossRef](#)]
8. Kumar, A.; Mishra, B.; Tripathi, B.P. Polydopamine assisted synthesis of ultrafine silver nanoparticles for heterogeneous catalysis and water remediation. *Nano-Struct. Nano-Objects* **2020**, *23*, 100489. [[CrossRef](#)]
9. Rauf, M.A.; Ashraf, S.S. Fundamental principles and application of heterogeneous photocatalytic degradation of dyes in solution. *Chem. Eng. J.* **2009**, *151*, 10–18. [[CrossRef](#)]
10. Jo, W.-K.; Kumar, S.; Isaacs, M.A.; Lee, A.F.; Karthikeyan, S. Cobalt promoted TiO₂/GO for the photocatalytic degradation of oxytetracycline and Congo Red. *Appl. Catal. B Environ.* **2017**, *201*, 159–168. [[CrossRef](#)]
11. Hama Aziz, K.H.; Miessner, H.; Mueller, S.; Mahyar, A.; Kalass, D.; Moeller, D.; Khorshid, I.; Rashid, M.A.M. Comparative study on 2,4-dichlorophenoxyacetic acid and 2,4-dichlorophenol removal from aqueous solutions via ozonation, photocatalysis and non-thermal plasma using a planar falling film reactor. *J. Hazard. Mater.* **2018**, *343*, 107–115. [[CrossRef](#)] [[PubMed](#)]

12. Dabhane, H.; Chatur, S.; Jadhav, G.; Tambade, P.; Medhane, V. Phytogetic synthesis of gold nanoparticles and applications for removal of methylene blue dye: A review. *Environ. Chem. Ecotoxicol.* **2021**, *3*, 160–171. [[CrossRef](#)]
13. Rajasekar, R.; Samuel, M.; Edison, T.N.J.I.; Raman, N. Sustainable synthesis of silver nanoparticles using *Alstonia scholaris* for enhanced catalytic degradation of methylene blue. *J. Mol. Struct.* **2021**, *1246*, 131208. [[CrossRef](#)]
14. Kora, A.J.; Rastogi, L. Catalytic degradation of anthropogenic dye pollutants using palladium nanoparticles synthesized by gum olibanum, a glucuronoarabinogalactan biopolymer. *Ind. Crops Prod.* **2016**, *81*, 1–10. [[CrossRef](#)]
15. Edison, T.N.J.I.; Atchudan, R.; Karthik, N.; Balaji, J.; Xiong, D.; Lee, Y.R. Catalytic degradation of organic dyes using green synthesized N-doped carbon supported silver nanoparticles. *Fuel* **2020**, *280*, 118682. [[CrossRef](#)]
16. Bolla, P.A.; Huggias, S.; Serradell, M.A.; Ruggera, J.F.; Casella, M.L. Synthesis and Catalytic Application of Silver Nanoparticles Supported on *Lactobacillus kefir* S-Layer Proteins. *Nanomaterials* **2020**, *10*, 2322. [[CrossRef](#)]
17. Saha, J.; Begum, A.; Mukherjee, A.; Kumar, S. A novel green synthesis of silver nanoparticles and their catalytic action in reduction of Methylene Blue dye. *Sustain. Environ. Res.* **2017**, *27*, 245–250. [[CrossRef](#)]
18. Alshorifi, F.T.; Alswat, A.A.; Mannaa, M.A.; Alotaibi, M.T.; El-Bahy, S.M.; Salama, R.S. Facile and Green Synthesis of Silver Quantum Dots Immobilized onto a Polymeric CTS–PEO Blend for the Photocatalytic Degradation of p-Nitrophenol. *ACS Omega* **2021**, *6*, 30432–30441. [[CrossRef](#)]
19. El-Yazeed, W.S.A.; El-Hakam, S.A.; Salama, R.S.; Ibrahim, A.A.; Ahmed, A.I. Ag–PMA supported on MCM-41: Surface Acidity and Catalytic Activity. *J. Sol-Gel Sci. Technol.* **2022**, *102*, 387–399. [[CrossRef](#)]
20. Wu, Y.; Wang, Z.; Chen, S.; Wu, J.; Guo, X.; Liu, Z. One-step hydrothermal synthesis of silver nanoparticles loaded on N-doped carbon and application for catalytic reduction of 4-nitrophenol. *RSC Adv.* **2015**, *5*, 87151–87156. [[CrossRef](#)]
21. Yuan, W.; Jiang, G.; Che, J.; Qi, X.; Xu, R.; Chang, M.W.; Chen, Y.; Lim, S.Y.; Dai, J.; Chan-Park, M.B. Deposition of Silver Nanoparticles on Multiwalled Carbon Nanotubes Grafted with Hyperbranched Poly(amidoamine) and Their Antimicrobial Effects. *J. Phys. Chem. C* **2008**, *112*, 18754–18759. [[CrossRef](#)]
22. Jahanbakhshi, M.; Habibi, B. A novel and facile synthesis of carbon quantum dots via salep hydrothermal treatment as the silver nanoparticles support: Application to electroanalytical determination of H₂O₂ in fetal bovine serum. *Biosens. Bioelectron.* **2016**, *81*, 143–150. [[CrossRef](#)] [[PubMed](#)]
23. Lellis, B.; Fávoro-Polonio, C.Z.; Pamphile, J.A.; Polonio, J.C. Effects of textile dyes on health and the environment and bioremediation potential of living organisms. *Biotechnol. Res. Innov.* **2019**, *3*, 275–290. [[CrossRef](#)]
24. Al-Tohamy, R.; Ali, S.S.; Li, F.; Okasha, K.M.; Mahmoud, Y.A.G.; Elsamahy, T.; Jiao, H.; Fu, Y.; Sun, J. A critical review on the treatment of dye-containing wastewater: Ecotoxicological and health concerns of textile dyes and possible remediation approaches for environmental safety. *Ecotoxicol. Environ. Saf.* **2022**, *231*, 113160. [[CrossRef](#)]
25. Saravanan, R.; Karthikeyan, S.; Gupta, V.K.; Sekaran, G.; Narayanan, V.; Stephen, A. Enhanced photocatalytic activity of ZnO/CuO nanocomposite for the degradation of textile dye on visible light illumination. *Mater. Sci. Eng. C* **2013**, *33*, 91–98. [[CrossRef](#)]
26. Eljiedi, A.A.A.; Kamari, A. Removal of methyl orange and methylene blue dyes from aqueous solution using lala clam (*Orbicularia orbiculata*) shell. *AIP Conf. Proc.* **2017**, *1847*, 040003. [[CrossRef](#)]
27. Su, Y.; Shi, B.; Liao, S.; Zhao, J.; Chen, L.; Zhao, S. Silver Nanoparticles/N-Doped Carbon-Dots Nanocomposites Derived from *Siraitia Grosvenorii* and Its Logic Gate and Surface-Enhanced Raman Scattering Characteristics. *ACS Sustain. Chem. Eng.* **2016**, *4*, 1728–1735. [[CrossRef](#)]
28. Zheng, M.; Wang, C.; Wang, Y.; Wei, W.; Ma, S.; Sun, X.; He, J. Green synthesis of carbon dots functionalized silver nanoparticles for the colorimetric detection of phoxim. *Talanta* **2018**, *185*, 309–315. [[CrossRef](#)]
29. Beiraghi, A.; Najibi-Gehraz, S.A. Carbon dots-modified silver nanoparticles as a new colorimetric sensor for selective determination of cupric ions. *Sens. Actuators B Chem.* **2017**, *253*, 342–351. [[CrossRef](#)]
30. Wei, X.; Cheng, F.; Yao, Y.; Yi, X.; Wei, B.; Li, H.; Wu, Y.; He, J. Facile synthesis of a carbon dots and silver nanoparticles (CDs/AgNPs) composite for antibacterial application. *RSC Adv.* **2021**, *11*, 18417–18422. [[CrossRef](#)]
31. Li, H.; Huang, J.; Lu, F.; Liu, Y.; Song, Y.; Sun, Y.; Zhong, J.; Huang, H.; Wang, Y.; Li, S.; et al. Impacts of Carbon Dots on Rice Plants: Boosting the Growth and Improving the Disease Resistance. *ACS Appl. Bio Mater.* **2018**, *1*, 663–672. [[CrossRef](#)] [[PubMed](#)]
32. Atchudan, R.; Edison, T.N.J.I.; Aseer, K.R.; Perumal, S.; Karthik, N.; Lee, Y.R. Highly fluorescent nitrogen-doped carbon dots derived from *Phyllanthus acidus* utilized as a fluorescent probe for label-free selective detection of Fe³⁺ ions, live cell imaging and fluorescent ink. *Biosens. Bioelectron.* **2018**, *99*, 303–311. [[CrossRef](#)] [[PubMed](#)]
33. Salama, R.S.; El-Sayed, E.-S.M.; El-Bahy, S.M.; Awad, F.S. Silver nanoparticles supported on UiO-66 (Zr): As an efficient and recyclable heterogeneous catalyst and efficient adsorbent for removal of indigo carmine. *Colloids Surf. A Physicochem. Eng. Asp.* **2021**, *626*, 127089. [[CrossRef](#)]
34. Atchudan, R.; Edison, T.N.J.I.; Chakradhar, D.; Perumal, S.; Shim, J.-J.; Lee, Y.R. Facile green synthesis of nitrogen-doped carbon dots using *Chionanthus retusus* fruit extract and investigation of their suitability for metal ion sensing and biological applications. *Sens. Actuators B Chem.* **2017**, *246*, 497–509. [[CrossRef](#)]
35. Atchudan, R.; Edison, T.N.J.I.; Lee, Y.R. Nitrogen-doped carbon dots originating from unripe peach for fluorescent bioimaging and electrocatalytic oxygen reduction reaction. *J. Colloid Interface Sci.* **2016**, *482*, 8–18. [[CrossRef](#)]

36. Atchudan, R.; Perumal, S.; Edison, T.N.J.I.; Albasher, G.; Sundramoorthy, A.K.; Vinodh, R.; Lee, Y.R. Lotus-biowaste derived sulfur/nitrogen-codoped porous carbon as an eco-friendly electrocatalyst for clean energy harvesting. *Environ. Res.* **2022**, *214*, 113910. [[CrossRef](#)] [[PubMed](#)]
37. Atchudan, R.; Chandra Kishore, S.; Gangadaran, P.; Jebakumar Immanuel Edison, T.N.; Perumal, S.; Rajendran, R.L.; Alagan, M.; Al-Rashed, S.; Ahn, B.-C.; Lee, Y.R. Tunable fluorescent carbon dots from biowaste as fluorescence ink and imaging human normal and cancer cells. *Environ. Res.* **2022**, *204*, 112365. [[CrossRef](#)] [[PubMed](#)]
38. Dager, A.; Baliyan, A.; Kurosu, S.; Maekawa, T.; Tachibana, M. Ultrafast synthesis of carbon quantum dots from fenugreek seeds using microwave plasma enhanced decomposition: Application of C-QDs to grow fluorescent protein crystals. *Sci. Rep.* **2020**, *10*, 12333. [[CrossRef](#)] [[PubMed](#)]
39. Liu, T.; Pang, Q.; Mai, K.; He, X.; Xu, L.; Zhou, F.; Liu, Y. Silver nanoparticle@carbon quantum dot composite as an antibacterial agent. *RSC Adv.* **2022**, *12*, 9621–9627. [[CrossRef](#)]
40. Atchudan, R.; Jebakumar Immanuel Edison, T.N.; Perumal, S.; Vinodh, R.; Babu, R.S.; Sundramoorthy, A.K.; Renita, A.A.; Lee, Y.R. Facile synthesis of nitrogen-doped porous carbon materials using waste biomass for energy storage applications. *Chemosphere* **2022**, *289*, 133225. [[CrossRef](#)]
41. Jyoti, K.; Singh, A. Green synthesis of nanostructured silver particles and their catalytic application in dye degradation. *J. Genet. Eng. Biotechnol.* **2016**, *14*, 311–317. [[CrossRef](#)] [[PubMed](#)]
42. Kim, B.; Song, W.C.; Park, S.Y.; Park, G. Green Synthesis of Silver and Gold Nanoparticles via Sargassum serratifolium Extract for Catalytic Reduction of Organic Dyes. *Catalysts* **2021**, *11*, 347. [[CrossRef](#)]
43. Luong, T.H.V.; Nguyen, T.H.T.; Nguyen, B.V.; Nguyen, N.K.; Nguyen, T.Q.C.; Dang, G.H. Efficient degradation of methyl orange and methylene blue in aqueous solution using a novel Fenton-like catalyst of CuCo-ZIFs. *Green Process. Synth.* **2022**, *11*, 71–83. [[CrossRef](#)]
44. Somasundaram, C.K.; Atchudan, R.; Edison, T.N.J.I.; Perumal, S.; Vinodh, R.; Sundramoorthy, A.K.; Babu, R.S.; Alagan, M.; Lee, Y.R. Sustainable Synthesis of Silver Nanoparticles Using Marine Algae for Catalytic Degradation of Methylene Blue. *Catalysts* **2021**, *11*, 1377. [[CrossRef](#)]
45. Edison, T.N.J.I.; Atchudan, R.; Sethuraman, M.G.; Lee, Y.R. Reductive-degradation of carcinogenic azo dyes using Anacardium occidentale testa derived silver nanoparticles. *J. Photochem. Photobiol. B Biol.* **2016**, *162*, 604–610. [[CrossRef](#)]
46. Edison, T.N.J.I.; Lee, Y.R.; Sethuraman, M.G. Green synthesis of silver nanoparticles using Terminalia cuneata and its catalytic action in reduction of direct yellow-12 dye. *Spectrochim. Acta Part A Mol. Biomol. Spectrosc.* **2016**, *161*, 122–129. [[CrossRef](#)]
47. Edison, T.N.J.I.; Atchudan, R.; Kamal, C.; Lee, Y.R. Caulerpa racemosa: A marine green alga for eco-friendly synthesis of silver nanoparticles and its catalytic degradation of methylene blue. *Bioprocess Biosyst. Eng.* **2016**, *39*, 1401–1408. [[CrossRef](#)]
48. Suvith, V.S.; Philip, D. Catalytic degradation of methylene blue using biosynthesized gold and silver nanoparticles. *Spectrochim. Acta Part A Mol. Biomol. Spectrosc.* **2014**, *118*, 526–532. [[CrossRef](#)]
49. Khodadadi, B.; Bordbar, M.; Nasrollahzadeh, M. Achillea millefolium L. extract mediated green synthesis of waste peach kernel shell supported silver nanoparticles: Application of the nanoparticles for catalytic reduction of a variety of dyes in water. *J. Colloid Interface Sci.* **2017**, *493*, 85–93. [[CrossRef](#)]
50. Hamedi, S.; Shojaosadati, S.A.; Mohammadi, A. Evaluation of the catalytic, antibacterial and anti-biofilm activities of the Convolvulus arvensis extract functionalized silver nanoparticles. *J. Photochem. Photobiol. B Biol.* **2017**, *167*, 36–44. [[CrossRef](#)]
51. Amjad, U.-E.-S.; Sherin, L.; Zafar, M.F.; Mustafa, M. Comparative Study on the Catalytic Degradation of Methyl Orange by Silver Nanoparticles Synthesized by Solution Combustion and Green Synthesis Method. *Arab. J. Sci. Eng.* **2019**, *44*, 9851–9857. [[CrossRef](#)]
52. Nagar, N.; Devra, V. A kinetic study on the degradation and biodegradability of silver nanoparticles catalyzed Methyl Orange and textile effluents. *Heliyon* **2019**, *5*, e01356. [[CrossRef](#)] [[PubMed](#)]
53. Bhankhar, A.; Giri, M.; Yadav, K.; Jaggi, N. Study on degradation of methyl orange-an azo dye by silver nanoparticles using UV-Visible spectroscopy. *Indian J. Phys.* **2014**, *88*, 1191–1196. [[CrossRef](#)]